Supplemental Notes

Note S1: Hashing of white and brown preadipocytes using oligo-conjugated hashtag antibodies

Cell hashing enables pooling of all samples prior to loading them onto a single 10X chromium controller lane, thereby enabling combined library preparation and sequencing of all samples to eliminate potential "batch" artifacts. During single-cell suspension preparation of white and brown preadipocytes for downstream scRNA-seq, we split each preadipocyte type into two individual microcentrifuge tubes for a total of four working samples. Brown preadipocytes were labelled with Hashtag-A0251 and A0252 antibodies, and white preadipocytes with A0253 and A0254 antibodies (Supplemental Table S1A). By sequencing these hashtag antibodies alongside the cellular transcriptome, we assigned each cell to its sample of origin, and identified doublets originating from multiple samples. Hashtag-antibody library was counted using the CITE-seq-Count workflow (10.5281/zenodo.2585469) and demultiplexed using the Seurat function 'MULTIseqDemux'. Demultiplexing pipeline identified 143 negative barcodes, 532 doublet barcodes, and 6918 cell-containing barcodes. As expected, every cell-containing barcode had highly positive and specific expression of only a single hashtag antibody, every doublet had marked expression for a combination of two antibodies, and negatives had very low expression for all antibodies (Supplemental Fig. S1A). While hashtag UMI counts revealed enrichment of protein targets in brown preadipocytes (Supplemental Fig. S1B, two-sided t-test), there was sufficient detection in both cell-types to enable robust cellular demultiplexing (Supplemental Fig. S1A).

Labeling protocol: For staining cells with hashtag antibodies, we followed supplier's protocol (https://www.protocols.io/view/cell-hashing-nfzdbp6). Briefly, cells were harvested from a single 100 mm cell-culture dish and suspended in 100 µl of cell staining buffer in 2 ml low bind tubes. 5 µl of Human TruStain FcX™ Fc Blocking reagent was then added, and cells were incubated for 10 minutes at 4°C. 0.5

ug of a unique Cell Hashing antibody was added to each tube and cells were incubate for 30 minutes at 4°C. Cells were washed with 1 mL of cell staining buffer for 3 times by centrifuging at 1200 rpm for 4 minutes at 4°C. Finally, cells were suspended in PBS and 0.04% BSA at ~ 1000 cells/uL for downstream 10X sequencing.

Note S2: Validation of scRNA-seq marker genes in recovering brown preadipocyte heterogeneity using smFISH

scRNA-seq of brown preadipocytes revealed existence of two distinct cell-types (Fig. 1B) marked by differential expression of several genes (Supplemental Table S1). We used single-molecule fluorescent in situ hybridization (smFISH) imaging to validate the differential expression of these genes in situ. Specifically, we targeted cluster-2 enriched gene *MMP1* for smFISH by designing short oligonucleotide probes complementary to the coding region of this gene (see Methods). Quantitative spot counting analysis, followed by gaussian mixture model fitting identified a 2-component bimodal distribution as the best fit (Supplemental Fig. S3, mean cluster 1 = 43 transcripts/cell, mean cluster 2 = 222 transcripts/cell), thereby corroborating the observation of two types of brown preadipocytes in our system. We used a likelihood ratio test of a 1-component fit against 2-component fit to determine which model best fits the data. This test yielded a p-value of 0.002 for the goodness of fit assessment between the two models, suggesting that the 2-component model is a more accurate approximation than the 1-component model for describing the parametric space of the observed distribution. We then used a 2-component negative binomial model to fit the count distributions, which is commonly used in single-cell RNA-seq measurements (Hafemeister and Satija 2019). The negative binomial model yielded similar cluster distribution, with mean transcripts per cell of 45 for cluster 1 and 174 for cluster 2, suggesting that our findings are independent of the distribution used.

Note S3: Investigating lack of differential enrichment of *ID1* gene in white nuclei

In our scRNA-seq dataset, *ID1* was the top differentially expressed (DE) gene in white preadipocyte over brown. However, in snRNA-seq dataset, *ID1* was not DE in white nuclei over brown nuclei. Comparison of transcript abundance for *ID1* across scRNA-seq and snRNA-seq in white preadipocytes revealed a significantly higher number of UMIs in scRNA-seq, even at a shallower sequencing depth (50,000 reads vs 75,000 reads; Supplemental Fig. S5A).

To better understand the lack of DE of *ID1* in single nuclei, we compared the transcript abundance (UMI count) in nuclei to the logFC in nuclei for all genes that were detected as DE in white preadipocytes using scRNA-seq (logFC>0.5). Among genes that were detected as DE in whole cells, any gene that had a transcript abundance below ~1 UMI in nuclei, were not detected as significantly DE in snRNA-seq (logFC < 0.5, Supplemental Fig. S5B). Meanwhile, multiple genes (*PLAU, TMEM119, HMOX1, CTHRC1,* and *NBL1*) with lower nuclear transcript abundance than *ID1*, were significantly differentially expressed in white nuclei (logFC > 0.5, Supplemental Fig. S5B). Moreover, these genes had a smaller effect size (logFC enrichment) than *ID1* in single cells. Together, these results suggest that *ID1* is not differentially enriched in nuclei but is differentially enriched in the cytoplasm between white and brown preadipocytes. In this analysis, we only considered exonic reads for this analysis to avoid transcript abundance inflation of long genes.

Note S4: Proliferating vs growth arrested cells in snRNA-seq and scRNA-seq white preadipocyte dataset

As highlighted in Fig. 6B UMAP visualization, both scRNA-seq and snRNA-seq white preadipocyte dataset (day-0) were cleaved into two halves. We investigated the differences between these two halves by manually annotating clusters as following (Supplemental Fig. S10A):

Cluster 0: day-20-differentiating-preadipocyte nuclei and cells

Cluster 1: day-20-adipocyte nuclei and cells

Cluster 2: top half of cleaved day-0-preadipocyte nuclei and cells

Cluster 3: bottom half of cleaved day-0-preadipocyte nuclei and cells

Cluster 4: day-20-cluster-2-nuclei

We normalized the data using *NormalizeData* command in Seurat and plotted expression profiles of proliferation and mitotic marker genes *PLK1*, *MYBL2*, *BUB1*, *MKI67*, *CDK1*, and *CCNB1* (Supplemental Fig. S10B to S10G). As expected, cluster 0 and 1 which primarily comprised of day-20 cells had no expression of proliferation markers, which is in line with their growth arrested behavior post adipogenic induction. However, prior to differentiation (day-0-preadipocytes), cells undergo cell cycle progression, thereby explaining the positive expression of proliferation marker genes in cluster 3. Cluster 2 cells were perhaps preadipocytes that underwent growth arrest due to contact inhibition during cell culture. Notably, even after 20 days of differentiation, a very small number of cells (cluster 4) were still highly proliferating, suggesting that these cells could be preadipocytes that never underwent growth arrest. We also calculated cell cycle phase scores based on canonical markers using the Cell-Cycle Scoring pipeline in Seurat and assigned either G1, G2M, or S Phase to each of these cells. As expected, most of the cells in clusters 0, 1, and 2 were in G1 phase as opposed to G2M and S phase in clusters 3 and 4 (Supplemental Fig. S10H).

Note S5: Outline of normalization strategy to correct for gene-length-based detection bias arising from including intronic reads

1. Rationale for Normalization

Multiple recent studies have demonstrated internal hybridization of poly(T) RT-primer to intronic poly(A) stretches as the primary mechanism for the capture and detection of intronic reads (La Manno et al. 2018; Patrick et al. 2020; Shulman and Elkon 2019). Assuming that all intronic reads are derived from such hybridization incidences, number of observed **intronic** UMIs for any gene g in a given nuclei can be estimated by the following equation:

$$p_i \times pA_g \times N_g = x_g \qquad \textit{Equation 1}$$

where p_i is the probability to capture an intronic read, pA_g are the number of poly(A) stretches in gene g and N_g is the true transcript abundance. Assuming that p_i is independent of gene g

$$N_g \propto \frac{x_g}{pA_g} \qquad \textit{Equation 2}$$

2. Estimating pA_g

pA_g can be modeled by the following equation, where pd is the number of poly(A) stretches per kilobase of the genic region in the human genome, and gl_g is the total length of the gene in kilobase, including introns and exons.

$$pA_g = pd \times gl_g \qquad \textit{Equation 3}$$

Since the poly(T) tail in 10x Chromium RT primer is 30-bp long, we assumed hybridization to occur between the poly(T) tail and a poly(A) stretch, if the poly(A) sequence is at least 15-bp long (50% of the poly(T) tail). We queried the GRCh38 human genome to get positions of all poly(A) tracts at least 15-bp long, without mismatch, and screened for overlaps between such poly(A) tracts and gene coordinates for all genes in the cellranger GRCh38-2020A reference (which includes lncRNAs). As expected, total number of poly(A) tracts were highly correlated with gene length (Spearman R = 0.82, p-value < 0.05,

Supplemental Fig. S6A) for each gene. We also calculated mean number of poly(A) tracts per Kbp for each gene, and estimated pd as the mean number of poly(A) tracts per Kbp across all genes, including zeroes (Supplemental Fig. S6B). Following this analysis, we estimated pd to be equal to 0.07.

We retrieved gene coordinates, strand, and gene length information using the GRCh38 gene annotation file downloaded from Gencode (Release 32). The same GTF was used for cellranger analysis. Briefly, each gene was first summarized by setting 3rd column in the GTF to **gene**, followed by calculation of gene length by subtracting the 5th and 4th columns.

3. Normalization Strategy

Based on *Equation 2*, we present a normalization framework to reduce the technical bias arising from comparisons of nuclear and cellular data upon inclusion of intronic reads. This normalization strategy is implemented on the count matrix generated using **only intronic reads**, for both scRNA-seq and snRNA-seq datasets, and provides a modified UMI count-abundance, taking gene-length into account, for each cell and nuclei, based on the following equations:

$$\overline{x_g} = \frac{x_g}{gl_g \times pd} \qquad \textit{Equation 4}$$

where x_g is the original UMI-count for gene g in a given cell/nuclei, and $\overline{x_g}$ is the modified UMI count after normalization for gene g in the same cell/nuclei. This modified intronic UMI-count is then added to the observed exonic UMI-count for each gene g in a given cell/nuclei and finally library-normalized as following:

$$\bar{z_g} = \log\left(\frac{\overline{x_g}+y_g}{N_i+N_e} \times e^4 + 1\right) \qquad \textit{Equation 5}$$

$$N_i = \sum_{g \in G} \overline{x_g} \qquad \textit{Equation 6}$$

$$N_e = \sum_{g \in G} y_g \qquad \textit{Equation 7}$$

where y_g is the original UMI-count for gene g using exonic reads, and $\bar{z_g}$ is the final log-normalized count used for downstream differential expression testing between cells and nuclei.

Note S6: Classification of differentially expressed genes in scRNA-seq dataset as marker genes

Fluorescent-activated cell sorting (FACS) has been instrumental in identifying lineage-specific preadipocyte marker genes in mice (Hepler et al. 2017). However, markers identified in mice are not comprehensively selective for humans (de Jong et al. 2015; Ferrero et al. 2020). We therefore sought to define a set of white-specific and brown-specific marker genes as well as a set of genes specifically expressed in cluster 1 and cluster 2. Using the identified list of differentially expressed genes (Supplemental Table S1B and S1C), we implemented stringent cutoff criteria with logFC > .8 in each cell-type, minimum detection of 60 % and maximum detection of 40% in the other cell-type, for classifying genes with highly enriched and specific expression as marker genes. On this basis, we recognized *NTNG1*, *RPL39L*, *PGF*, *LAMA4*, *BAALC*, *HIP1*, and *HAS2* as markers of white preadipocytes; *LIMCH1*, *LYPD1*, *RGS4*, *ITGBL1*, *CDH13*, and *COL4A2* as markers of brown preadipocytes in the human neck depot (Fig. 1B and Supplemental Table S1B). We also identified *KRT18*, *LUZP2*, *DLGAP1*, *SBSPON*, *MAP3K7CL*, and *NRXN3* as markers of brown cluster 1; *CTSK*, *BST2*, and *MOXD1* as markers of brown cluster 2 (Fig. 1B and Supplemental Table S1C).

Supplemental Tables

Supplemental Table S1: Analysis of white and brown preadipocyte scRNA-seq dataset

(A) Oligo-tagged hashtag antibodies used for sample multiplexing of white and brown preadipocyte for downstream scRNA seq

(B) DE genes between white and brown preadipocytes in scRNA-seq dataset (white vs brown test, logFC > 0 means enrichment in white preadipocytes)

(C) DE genes between brown cluster 1 and cluster 2 in scRNA-seq dataset (logFC > 0 means enrichment in brown cluster 1)

(D) Top 20 transcription factors (TF) identified in cluster 1 brown preadipocyte using ChEA3 tool for TF enrichment analysis (TFEA). Genes with logFC > 0 in Table C above were used as input for TFEA.

Supplemental Table S2: Analysis of white and brown preadipocyte snRNA-seq dataset

(A) Differential expression of genes in white and brown nuclei (white vs brown test, logFC > 0 means enrichment in white nuclei)

(B) DE genes between brown cluster 1 and cluster 2 in snRNA-seq dataset (logFC > 0 means enrichment in brown cluster 1)

Supplemental Figures

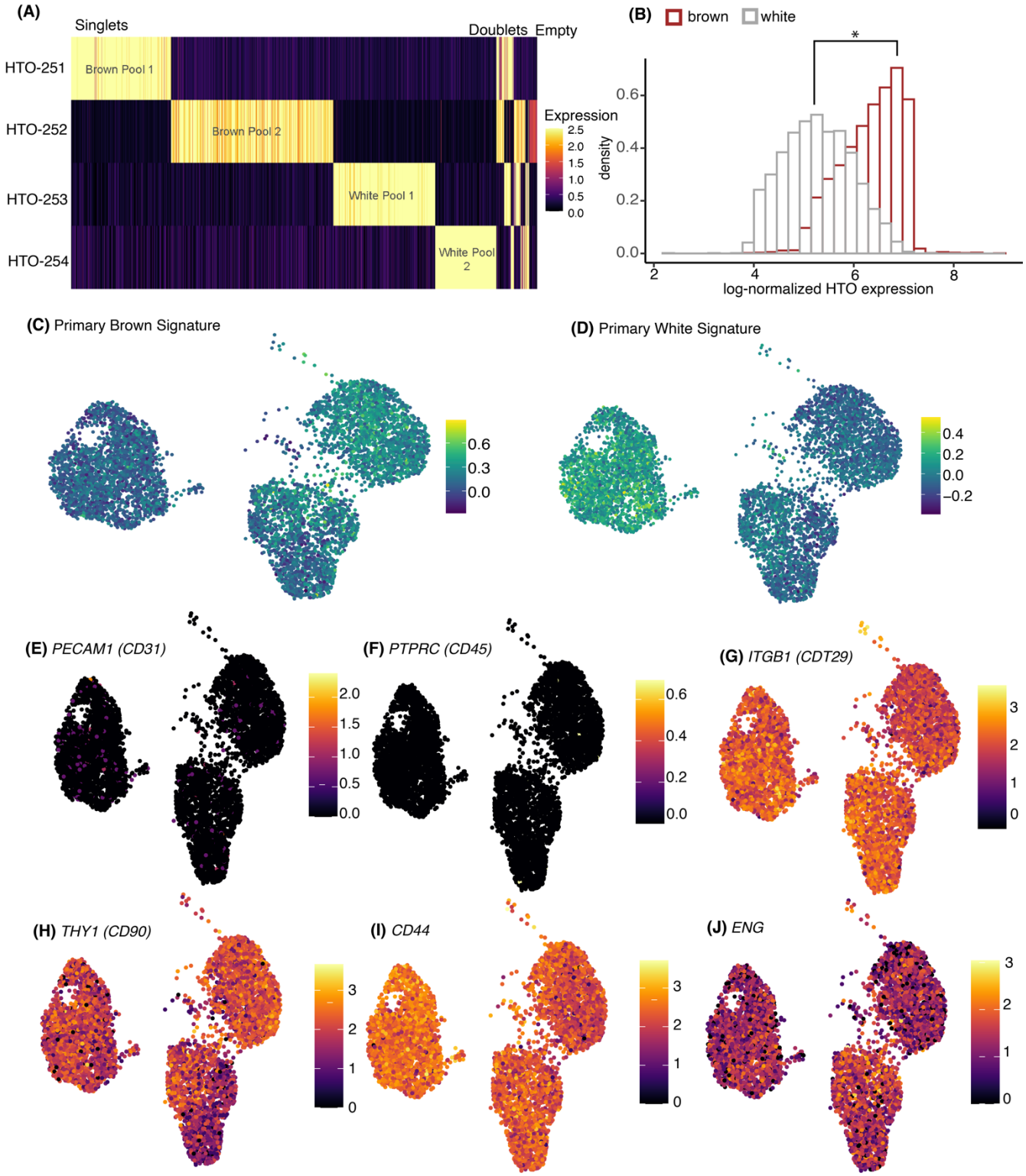

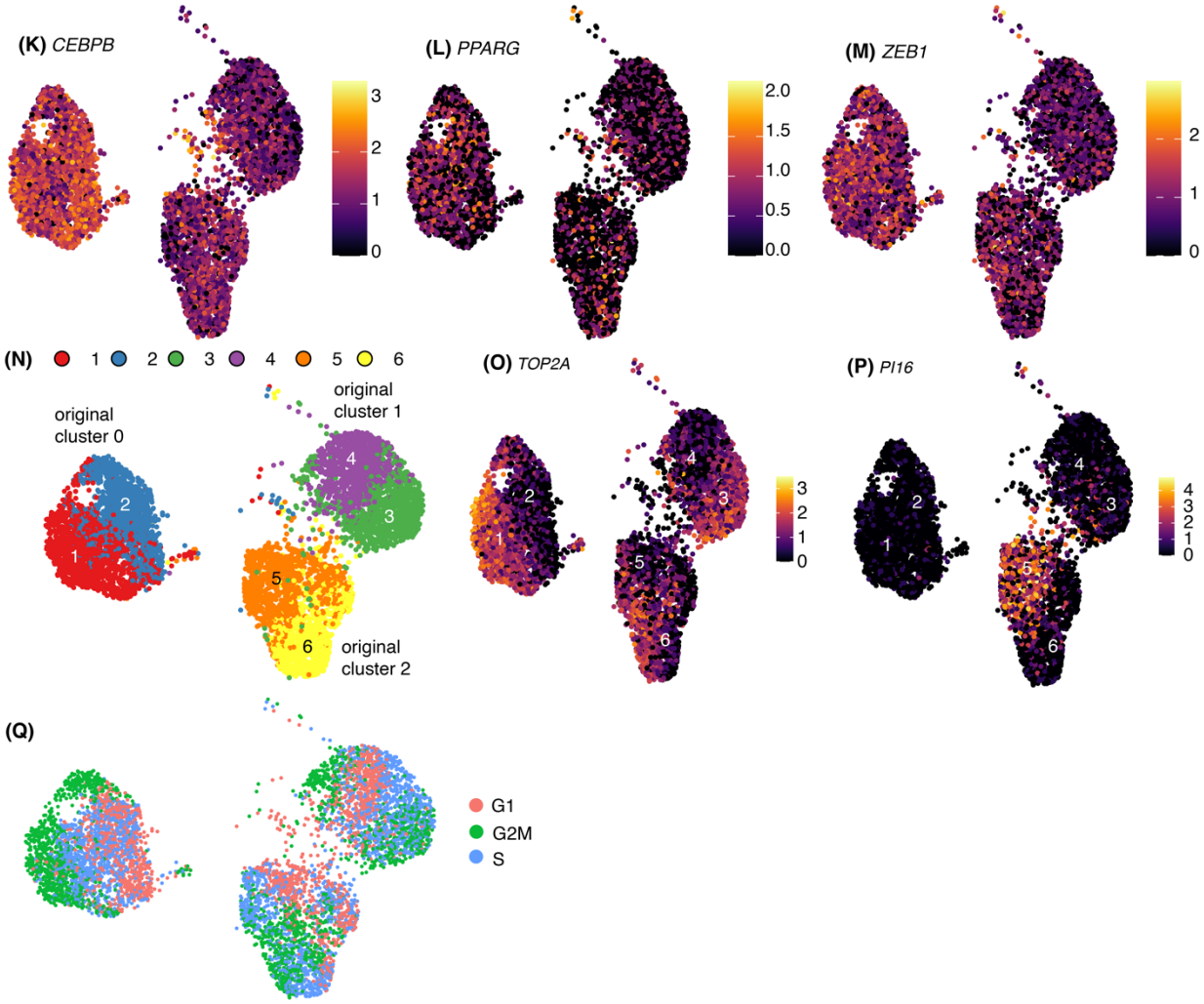

Supplemental Figure S1 (related to Result # 1 and Figure 1) Analysis of white and brown preadipocyte scRNA-seq dataset (A) Log-normalized expression of four hashtag antibodies used for multiplexing of white and brown preadipocytes (whole-cells). Each row marks the expression of a given antibody in 5000 randomly sampled barcodes (columns). Also see Note S1 and Supplemental Table S1A. **(B)** Distribution of normalized hashtag antibody expression in white and brown preadipocytes identified as singlets. Statistical testing was performed using a two-sided t-test. **(C) to (D)** Heatmap of transcriptional signature scores for white preadipocyte **(C)** and brown preadipocyte **(D)**, as plotted on the UMAP visualization of scRNA-seq preadipocyte data. Original signatures were defined using primary white and brown preadipocytes isolated from the same anatomical region as the in-vitro model system used in our study (see Methods). **(E) to (M)** Expression profiles of marker genes in scRNA-seq dataset. **(N)** Sub-clusters identified for each of the original cluster 0, 1, and 2 in Fig. 1A. **(O)** Expression profile of mitotic cell marker *TOP2A*, one of the top marker genes during sub-clustering of original clusters 0, and 1 in scRNA-seq dataset. **(P)** Expression profile of adipocyte progenitor marker *PI16*, the top marker gene during sub-clustering of original cluster 2 in scRNA-seq dataset. **(Q)** Cells annotated by cell-cycle phase as calculated using Seurat

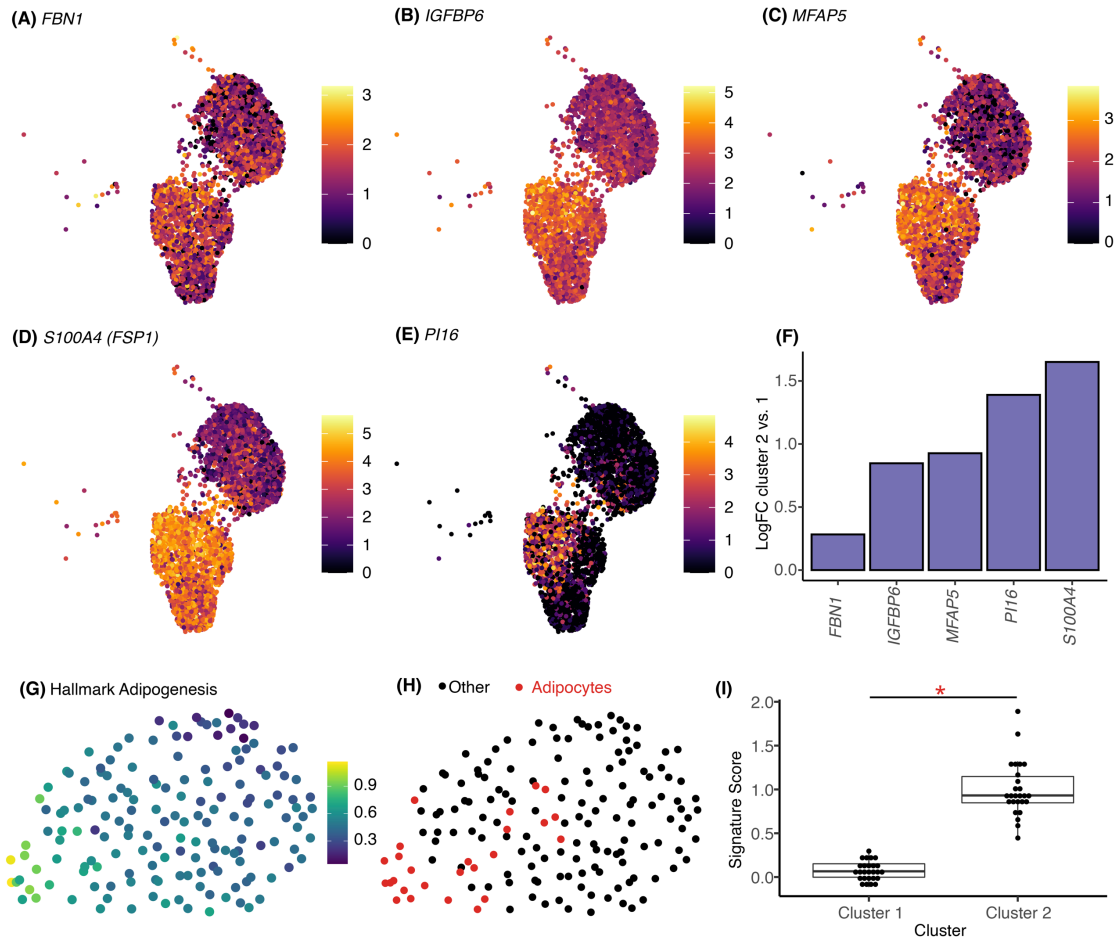

Supplemental Figure S2 (related to Result # 1 and Figure 1) Differential expression in brown preadipocyte scRNA-seq dataset between cluster 2 and cluster 1. (A) to (E) Expression profile of marker genes for Fsp1+ fibroblasts identified in (Vijay et al. 2020) **(F)** Log fold change values of the marker genes as calculated using cluster 2 vs cluster 1 differential expression test. All genes were significantly enriched in cluster 2 with FDR < 0.05. Also see Supplemental Table S1C. (**G)** Heatmap of Hallmark Adipogenesis signature defined in MSig database. The signature consists of genes up regulated during adipocyte differentiation. **(H)** Cells identified as mature adipocytes after unsupervised clustering in Seurat **(I)** Boxplot of transcriptional signature scores in mature adipocytes (highlighted in red in panel H). Signatures were defined for cluster 1 and cluster 2 cells using scRNA-seq dataset (see Supplemental Table S1C). Statistical testing was performed using two-sided Mann-Whitney U-test.

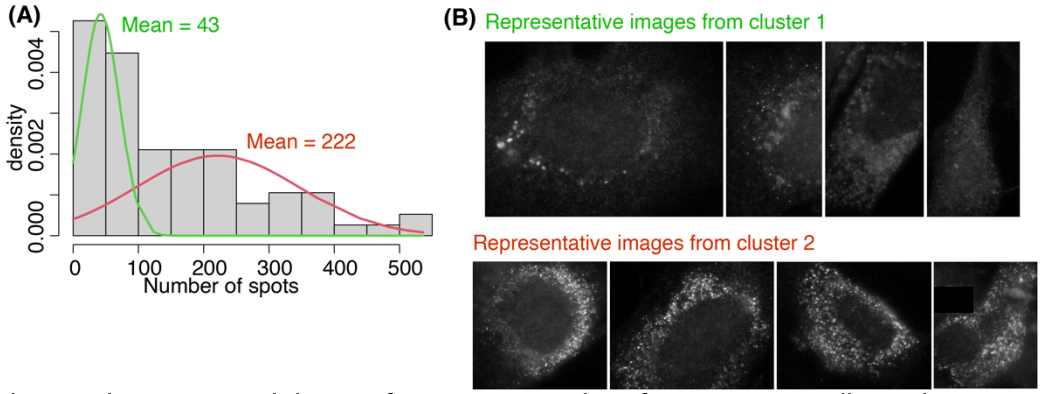

Supplemental Figure S3 Validation of scRNA-seq markers for recovering cell-type heterogeneity in brown preadipocytes using smFISH. (A) Distribution of number of *MMP1* mRNA spots per cell in brown preadipocytes. Overlaid gaussian distributions represent the 2-component fit identified using Gaussian finite mixture model fitting. **(B)** 4 representative images of cells from cluster 1 (mean = 43) and cluster 2 (mean = 222). Representative images are cells within +/- 7 transcript counts from the mean.

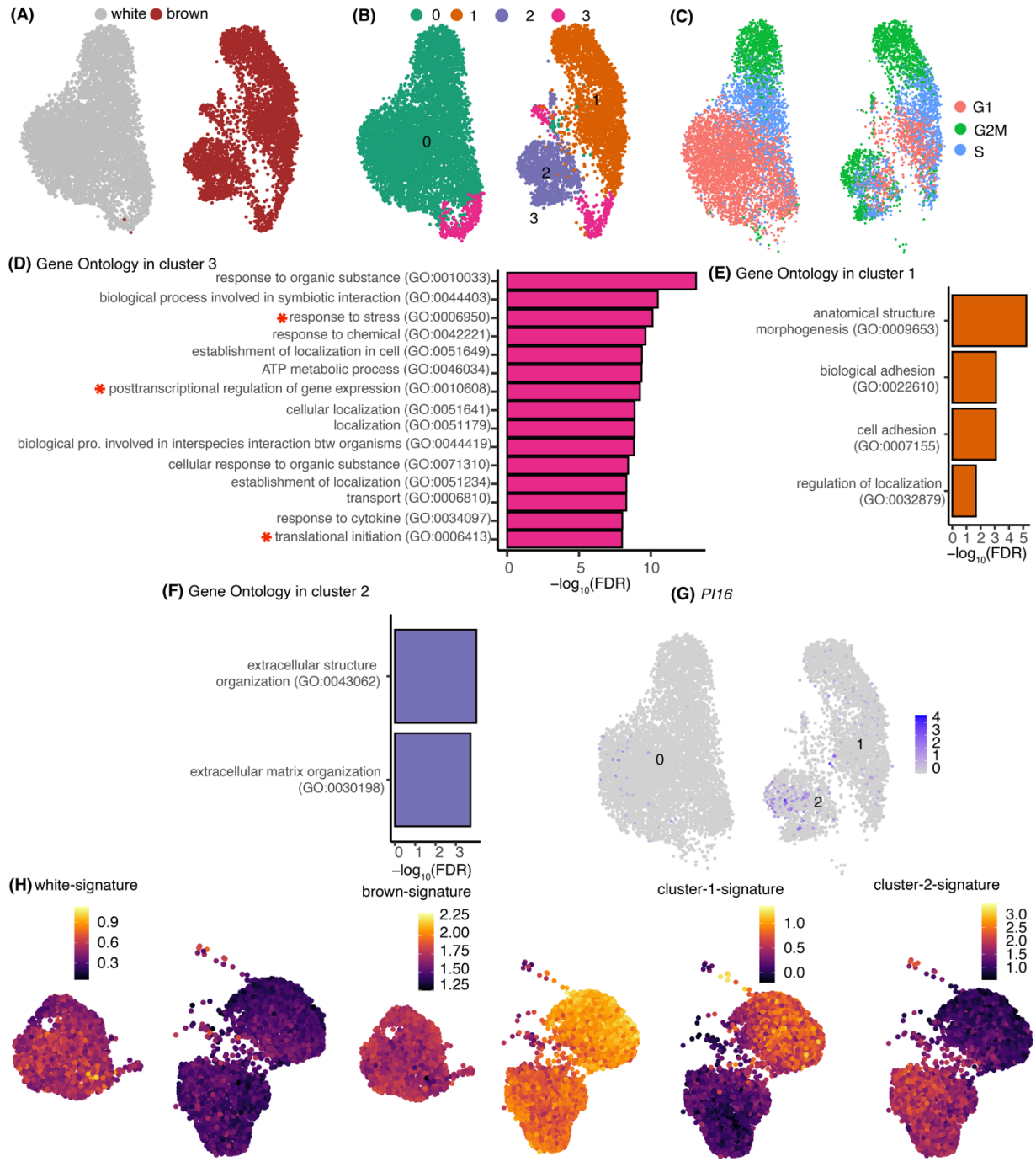

Supplemental Figure S4 (related to Result # 2 and Figure 2) Unsupervised clustering of white and brown preadipocytes snRNA-seq dataset (A) and (B) UMAP visualization of white and brown preadipocytes annotated either manually to reflect the sample of origin (A) or based on unsupervised clustering (B). **(C)** Cells annotated by cell-cycle phase as calculated using Seurat **(D)** Top gene ontology biological processes (BP) terms enriched in cluster 3 based on a cluster 3 vs. all DE test. Marked in red is the enrichment of BP terms because of stress response genes (response to stress), mitochondrial genes (ATP metabolic process), and ribosomal mRNA genes (translational initiation). Enrichment of mitochondrial and ribosomal mRNA genes indicates the presence of cellular background RNA contamination (see

Supplemental Fig. S7). **(E)** Top 10 gene ontology terms in brown cluster 1 in scRNA-seq dataset (Fig. 1C) that are also enriched in cluster 1 in snRNA-seq dataset. None of these top 10 GO terms were enriched in cluster 2 in snRNA-seq dataset. **(F)** Top 10 gene ontology terms in brown cluster 2 in scRNA-seq dataset (Fig. 1C) that are also enriched in cluster 2 in snRNA-seq dataset. None of these top 10 GO terms were enriched in cluster 1 in snRNA-seq dataset. **(G)** Expression profile of adipocyte progenitor marker *PI16* in snRNA-seq dataset. Also see Supplemental Fig. S1P. **(H)** Heatmap of transcriptional signature scores for white preadipocyte (white), brown preadipocyte (brown), brown preadipocyte cluster 1 (one), and brown preadipocyte cluster 2 (two) as plotted on the UMAP visualization of scRNA-seq data. Signatures were defined using snRNA-seq data using white vs brown, or cluster-1 vs cluster-2 differential expression testing.

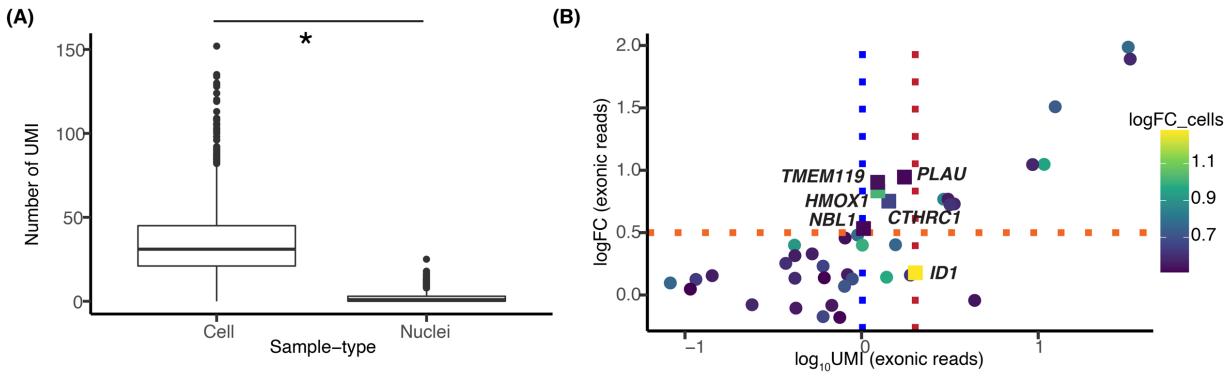

Supplemental Figure S5 Investigating lack of *ID1* DE in white nuclei over brown nuclei. (A) Boxplot of number of *ID1* UMIs detected in each cell or nuclei isolated from white preadipocyte. **(B)** Log-fold-change vs log-UMI counts in white nuclei when using only exonic reads, where each dot represents a white-preadipocyte-enriched gene (white vs brown DE test) detected using scRNA-seq dataset (Fig. 1A). Horizontal dotted line indicates logFC cutoff value of 0.5 used as a threshold for DE testing. All genes had a logFC > 0.5 in scRNA-seq dataset. Vertical blue dotted line indicates smallest mean UMI count at which a gene was detected to be differentially expressed. Vertical red dotted line indicates the mean UMI count for *ID1* gene. *ID1* gene is marked with a square, along with genes *TMEM119*, *PLAU*, *HMOX1*, *NBL1*, and *CTHRC1*.

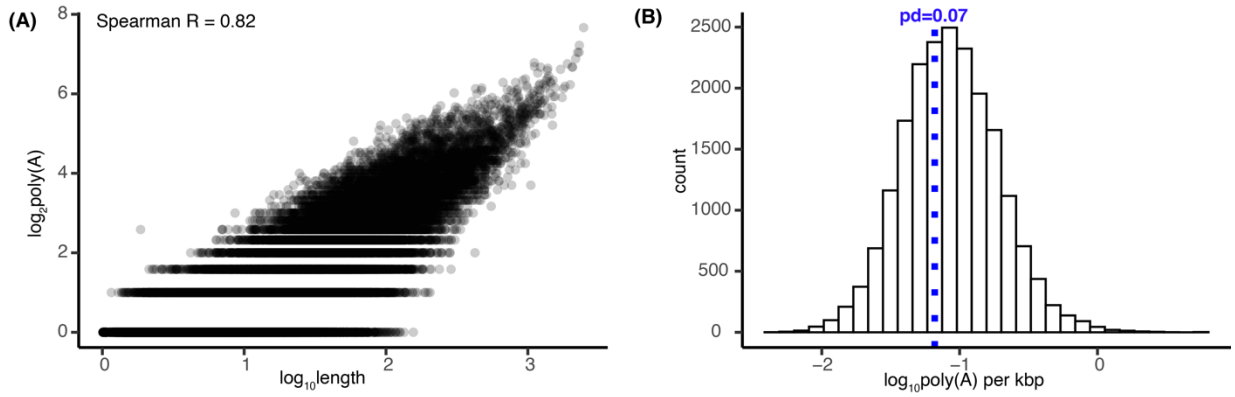

Supplemental Figure S6 (related to Note S5) Estimating poly(A)-tract density per Kbp in the genic region. (A) Scatter plot of total number of poly(A)-tracts (greater than 15-bp) plotted against gene length. Each dot is a gene in the GRCh38-2020A reference from cellranger analysis pipeline. **(B)** Distribution of mean number of poly(A)-tracts per Kbp for each gene in panel A. Blue dotted line indicates mean number of poly-A tracts per Kbp across all genes and is used to estimate *pd*=0.07. See Note S5 for details on normalization strategy.

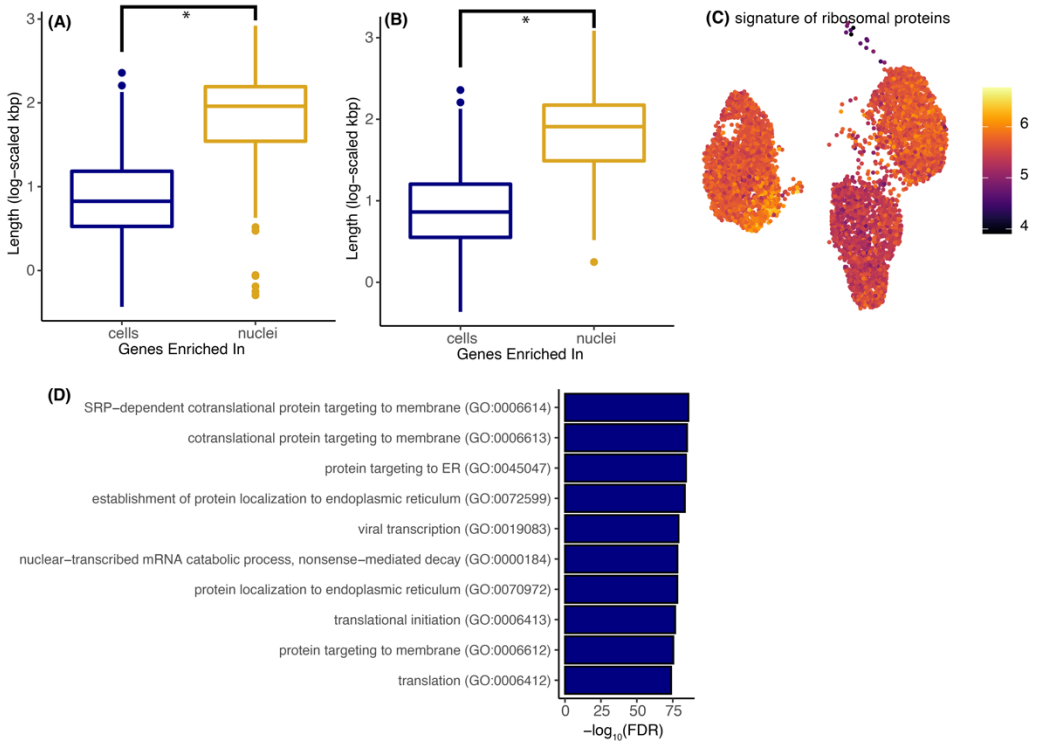

Supplemental Figure S7 (related to Result # 3 and Figure 3) Gene length-associated detection bias in snRNA-seq. (A) Distribution of gene length for genes enriched in cells (in blue) and nuclei (in yellow) with log fold-change > 1 and FDR < 0.05 including both intronic and exonic reads. Intronic UMI-count matrix was normalized to correct for gene length bias in both cells and nuclei (see Note S5). **(B)** Distribution of gene length for genes enriched in cells (in blue) and nuclei (in yellow) with log fold-change > 1 and FDR < 0.05 using only exonic reads. **(C)** Heatmap of transcriptional signature score defined using top 100 genes enriched in cells vs. nuclei in white preadipocytes based on log fold-change values after normalization. The scores are plotted on the 2D UMAP visualization of scRNA-seq preadipocyte data. **(D)** Top 10 gene ontology terms enriched in white cells as compared to white nuclei based on differential expression after normalization.

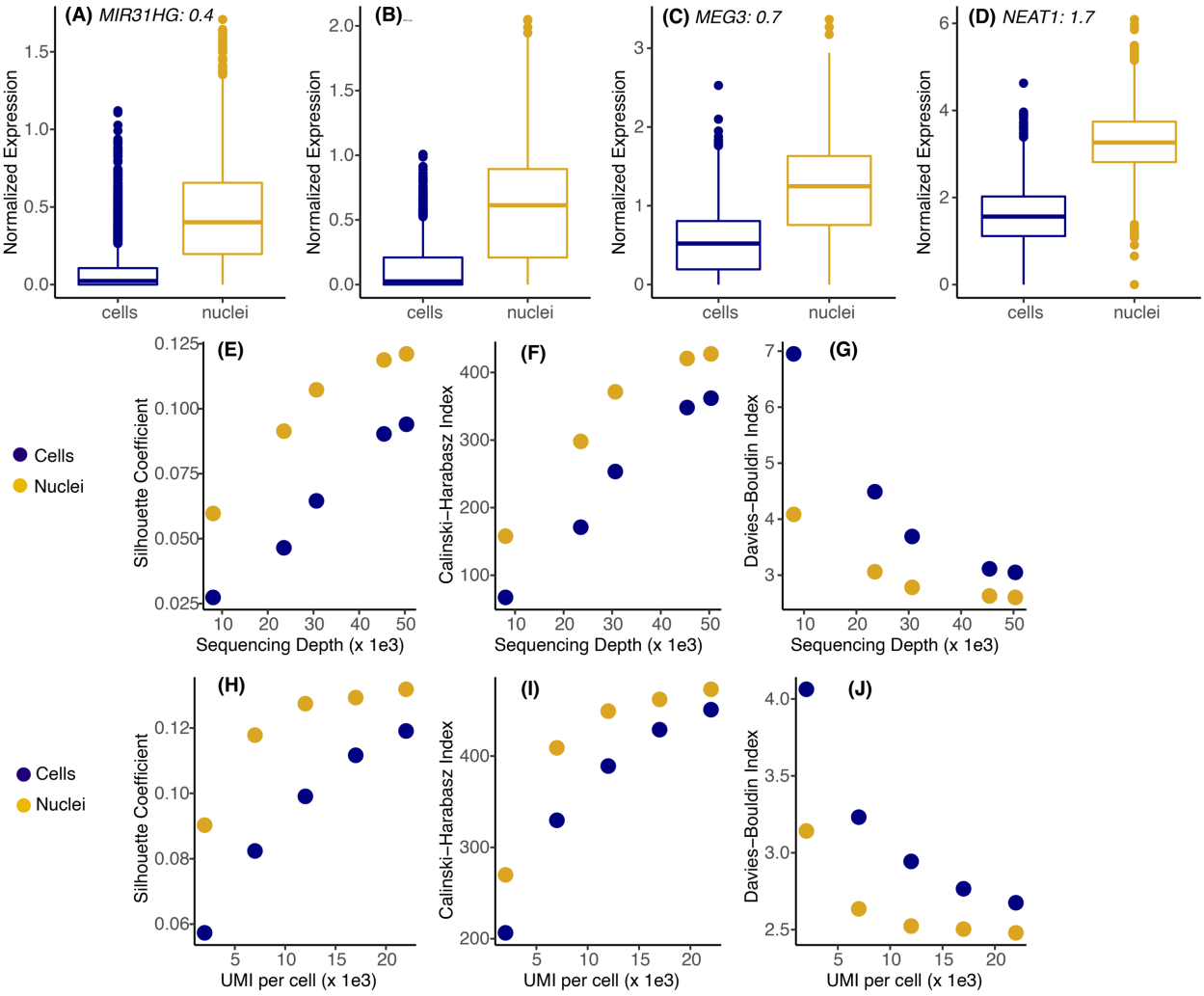

Supplemental Figure S8 (related to Result # 4 and Figure 4) Enrichment of lncRNAs in the nuclear transcriptome. (A) to (D) Expression of adipogenic regulatory lncRNAs in brown nuclei over brown whole cells. Black text indicates logFC value for brown nuclei vs. brown cells DE test with FDR < 0.05 after normalization. **(E) to (G)** Cluster separation resolution quantification between brown cluster 2 vs cluster 1 in scRNA-seq and snRNA-seq dataset. **Only lncRNAs were considered for PCA manifold generation.** Both datasets were subsampled to have the same number of cells/nuclei and same number of mean transcriptome mapped reads. **(H) to (J)** Similar analysis as panel (E) to (G) but normalization was performed to have the same number of UMI counts per cell/nuclei. A higher Silhouette coefficient and Calinski Harabasz and a lower Davies Bouldin index indicate superior cluster separation performance.

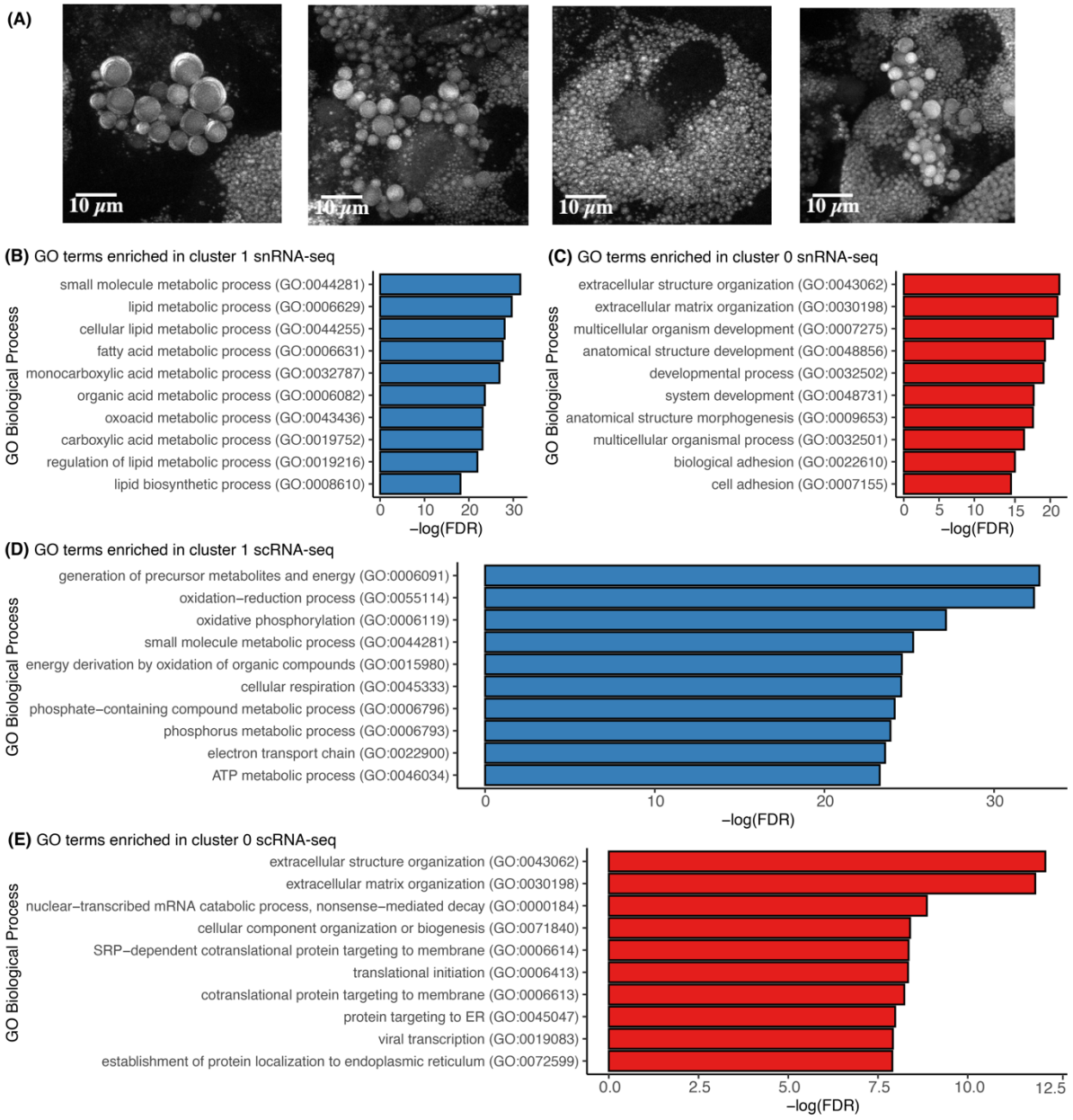

(F) *DHCR24; HIST2H2AA4; UHMK1; MGST3; PRDX6; TIMP4; COX7A2; NDUFA4; CD36; NDUFA1; UQCRB; COX6C; NDUFB9; STOM; COX8A; CRYAB; H2AFJ COX14; ATP5F1B; COX6A1; AC126365.1; NDUFV2; ATP5F1A; ECH1; APOE; APOC1; UQCR10*

Supplemental Figure S9 (related to Result # 5 and Figure 5) Comparative analysis of nuclear and whole-cell transcriptome at mature adipocyte stage (A) Coherent anti-stokes Raman imaging of human white preadipocytes differentiated for 20 days using a chemical adipogenic induction cocktail. The images were acquired at 2845 cm^{-1} wavenumber, which corresponds to the CH_3 peak present in lipids. Z-stacked images were acquired and the maximum intensity projection for each pixel was plotted. **(B) and (C)** Top 10 gene ontology terms enriched in cluster 1 (panel B) and cluster 0 (panel C) in **snRNA-seq dataset**. **(D) and (E)** Top 10 gene ontology terms enriched in cluster 1 (panel D) and cluster 0 (panel E) in **scRNA-seq dataset**. **(F)** List of 27 genes differentially enriched in cluster 1 (mature adipocytes) in scRNA-seq dataset but not differentially enriched in cluster 1 of snRNA-seq dataset

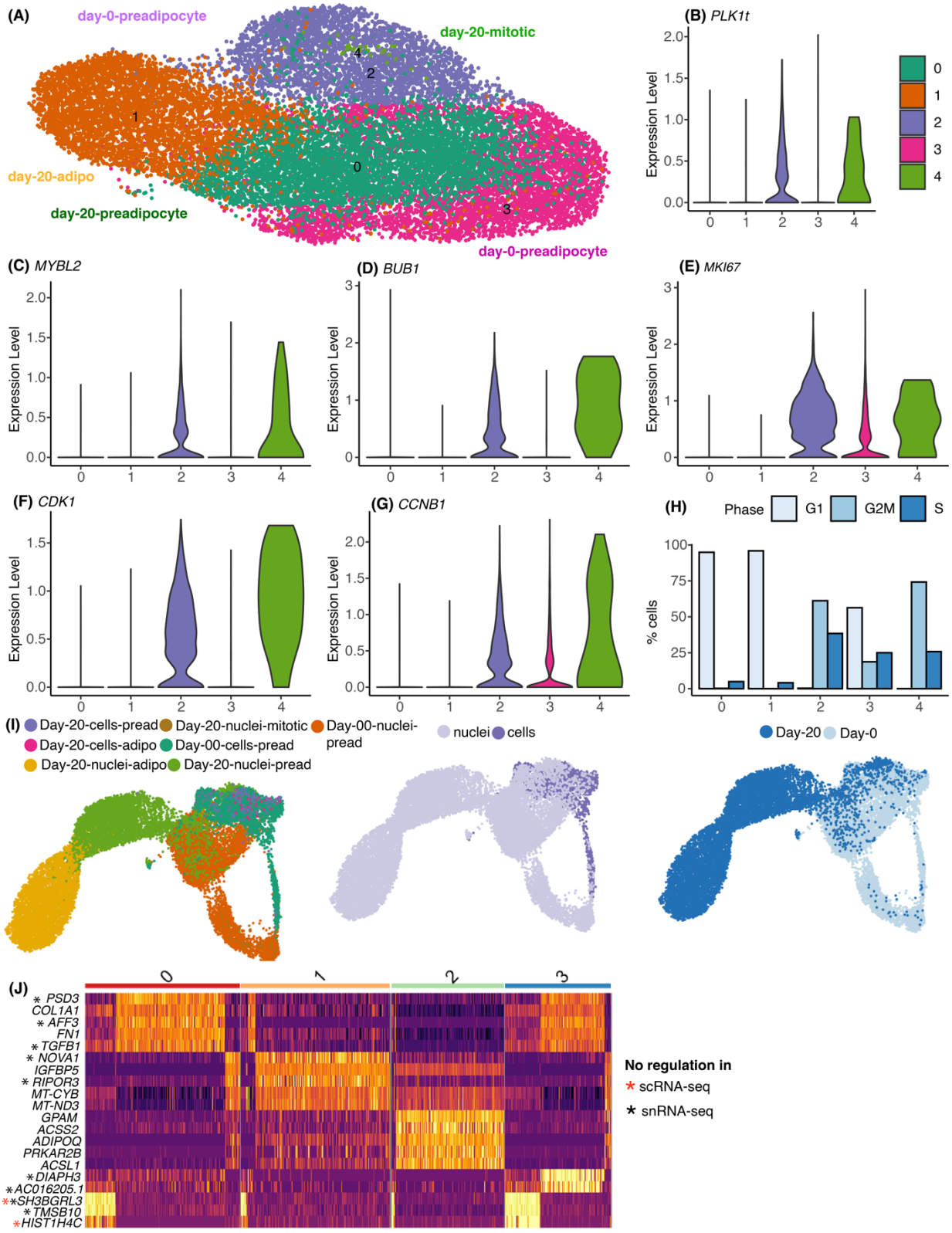

Supplemental Figure S10 (related to Note S4, Result # 6 and Figure 6): Proliferating vs growth arrested cells in snRNA-seq and scRNA-seq white preadipocyte dataset. (A) Supervised clustering of integrated

scRNA-seq and snRNA-seq white preadipocyte (day-0) and white adipocyte (day-20) dataset. See Note S4 for details regarding clustering scheme. **(B) to (G)** Violin plots of common proliferation and mitosis marker genes in clusters identified in panel (A). **(H)** Bar plot of distribution of cell cycle phase assignment in the clusters identified in panel (A). Y-axis plots the percent of cells belonging to different cell cycle phase for every cluster. See Note S4 for details regarding cell cycle phase assignment. **(I)** UMAP visualization of integrated white preadipocyte day-0 and day-20, scRNA-seq and snRNA-seq datasets. Cells are annotated by original clusters (left panel), sequencing technique (middle panel), and harvestation day (right panel). Integration was performed using Seurat v3. **(J)** Heat map of top 5 marker genes for each cluster identified using Seurat (Fig. 6C right-most panel), with genes as rows, and cells as columns. The color bar on top represents cluster assignment. All genes were differentially expressed in both scRNA-seq and snRNA-seq datasets, except for the ones marked in red or black (see Methods).

REFERENCES

de Jong JMA, Larsson O, Cannon B, Nedergaard J. 2015. A stringent validation of mouse adipose tissue identity markers. *Am J Physiol - Endocrinol Metab* **308**: E1085–E1105. https://pubmed.ncbi.nlm.nih.gov/25898951/ (Accessed October 21, 2020).

Ferrero R, Rainer P, Deplancke B. 2020. Toward a Consensus View of Mammalian Adipocyte Stem and Progenitor Cell Heterogeneity. *Trends Cell Biol* **30**: 937–950.

Hafemeister C, Satija R. 2019. Normalization and variance stabilization of single-cell RNA-seq data using regularized negative binomial regression. *Genome Biol* **20**: 1–15. https://genomebiology.biomedcentral.com/articles/10.1186/s13059-019-1874-1 (Accessed September 27, 2021).

Hepler C, Vishvanath L, Gupta RK. 2017. Sorting out adipocyte precursors and their role in physiology and disease. *Genes Dev* **31**: 127–140.

La Manno G, Soldatov R, Zeisel A, Braun E, Hochgerner H, Petukhov V, Lidschreiber K, Kastriti ME, Lönnerberg P, Furlan A, et al. 2018. RNA velocity of single cells. *Nature* **560**: 494–498. http://www.nature.com/articles/s41586-018-0414-6 (Accessed September 12, 2018).

Patrick R, Humphreys DT, Janbandhu V, Oshlack A, Ho JWK, Harvey RP, Lo KK. 2020. Sierra: Discovery of differential transcript usage from polyA-captured single-cell RNA-seq data. *Genome Biol* **21**: 167. https://genomebiology.biomedcentral.com/articles/10.1186/s13059-020-02071-7 (Accessed October 7, 2020).

Shulman ED, Elkon R. 2019. Cell-type-specific analysis of alternative polyadenylation using single-cell transcriptomics data. *Nucleic Acids Res* **47**: 10027–10039. https://academic.oup.com/nar/article/47/19/10027/5566587 (Accessed October 22, 2020).

Vijay J, Gauthier MF, Biswell RL, Louiselle DA, Johnston JJ, Cheung WA, Belden B, Pramatarova A, Biertho L, Gibson M, et al. 2020. Single-cell analysis of human adipose tissue identifies depot- and disease-specific cell types. *Nat Metab* **2**: 97–109.